Supporting Information:

Charge Transport and Rectification in Arrays of SAM-Based Tunneling Junctions

Christian A. Nijhuis, William F. Reus, Jabulani R. Barber, Michael D. Dickey, and George M. Whitesides[*]

Department of Chemistry and Chemical Biology, Harvard University, 12 Oxford St, Cambridge, MA 02138, USA

Corresponding author:

Tel.: 617 458 9430

Fax.: 617 458 9857

e-mail: gwhitesides@gmwgroup.harvard.edu

Nomenclature. We studied two different types of SAMs in this work: Ferrocene-(Fc) terminated SAMs of $SH(CH_2)_{11}Fc$ (which we abbreviate as $SC_{11}Fc$), and SAMs of n-alkanethiolates of $HS(CH_2)_{n-1}CH_3$ (which we abbreviate as $SC_{n-1}CH_3$; with n = 12, 14, 16, or 18). We use the general notation Ag^{TS}-$SC_{11}Fc$//Ga_2O_3/EGaIn to describe the junctions[1]: Here, Ag^{TS}-$SC_{11}Fc$ is a template-striped (TS) silver thin-film electrode supporting a SAM of $SC_{11}Fc$. We describe the interfaces with the symbols "-", which indicates a chemisorbed contact, "/", which indicates the interface of Ga_2O_3 and EGaIn, and "//", which indicates the presence of a non-covalent interface. The symbol V is defined as the difference in voltage between the two electrodes. We abbreviate polydimethylsiloxane as PDMS.

Electrical Properties of the Layer of Ga_2O_3. We performed two experiments to determine the resistance of the layer of Ga_2O_3 in our junctions. i) As reported before, we measured the resistance of the layer of Ga_2O_3 by contacting one copper wire (with a diameter of 80 μm) and the bulk of EGaIn with a second one, and that of bulk EGaIn by contacting bulk EGaIn with two copper wires.[2] This measurement indicated that the layer of Ga_2O_3 is a factor of ~65 more resistive than bulk EGaIn.2 ii) We contacted cone-shaped tips of Ga_2O_3/EGaIn to transparent electrodes of ITO (tin-doped indium oxide) while measuring the current in real time at an applied bias of 50 mV. We recorded optical micrographs through the transparent ITO to determine the size of the junctions. Figure S1 shows that the current increased (as expected) with the junction size, but suddenly increased by a factor of about ~100 at t = 340 s. This value of the current is similar to that of a circuit without the cone-shaped tip of Ga_2O_3/EGaIn, i.e., ITO contacted directly with a metal probe biased at 50 mV. We believe that this sudden increase in the current results from the formation of direct contact of bulk EGaIn with the ITO. In this particular circuit, the resistance of the layer of Ga_2O_3 varied between $10^3 – 10^4$ Ω depending on the size of the contact. The resistance of the short-circuited contact was 10^2 Ω; thus, we conclude that the layer of Ga_2O_3 in a typical junction is approximately two orders of magnitude greater than the resistance of the rest of the circuit, including the bulk EGaIn. Even for SAMs of $SC_{10}CH_3$ (the most conductive SAM we measured) current at 0.5 V was consistently less than 10^{-8} A, implying a minimum resistance of $5 \cdot 10^7$ Ω for these SAMs. Therefore, the layer of Ga_2O_3 in a typical SAM-based junction has a resistance at least three to four orders of magnitude less than that of the SAMs we measure. In our junctions, current through the circuit is limited by the SAM, not by the layer of Ga_2O_3.

By estimating the area of contact between Ga_2O_3 and ITO from the optical micrographs in Figure S1 and assuming that the thickness of the layer of Ga_2O_3 is 2 nm, we calculated a resistivity of $\rho = \sim 10^6$ Ωcm for the Ga_2O_3. Paterson et al.[3] reported a resistivity of $\rho = \sim 10^{10}$ Ωcm in the low-bias regime (0 V < *V* < 0.4 V) for a 10 nm-thick film of epitaxially grown Ga_2O_3 on GaAs. Since the native film of Ga_2O_3 on EGaIn forms spontaneously in air, it likely contains many more defects and is thus more conductive than an epitaxially grown film.

In order to establish the mechanism of charge-transport in Ga_2O_3, we contacted the layer of Ga_2O_3 on a drop of EGaIn using Cu wires, as described above, and performed measurements of charge-transport at various temperatures (Figure S2). Starting at 295 K, we incrementally decreased the temperature while measuring current vs. applied bias. At 260 K, the liquid EGaIn solidified, disturbing the contact between Cu and Ga_2O_3 and hindering further measurements. However, in the range of 295 – 260 K, we observed a strong dependence of current on temperature, indicating that charge-transport proceeds *via* a thermally activated process. We plan to report a detailed analysis of these results in a separate paper;[4] however, our observation of thermally activated charge-transport agrees with Paterson et al.,3 who reported that thermionic emission was the dominant mechanism of charge-transport through epitaxially grown films of Ga_2O_3 on GaAs.

Figure S1: The current measured as a function of time while contacting a cone-shaped tip of Ga_2O_3/EGaIn to ITO. At t = 5 s the tip contacted the ITO and allowed a current of 3.2 μA to flow. The current increased as the junction size increased (optical micrographs show the footprint of the junction, seen from below the ITO, at various times) until, at *t* = 340 s, the current suddenly increased to ~200 μA.

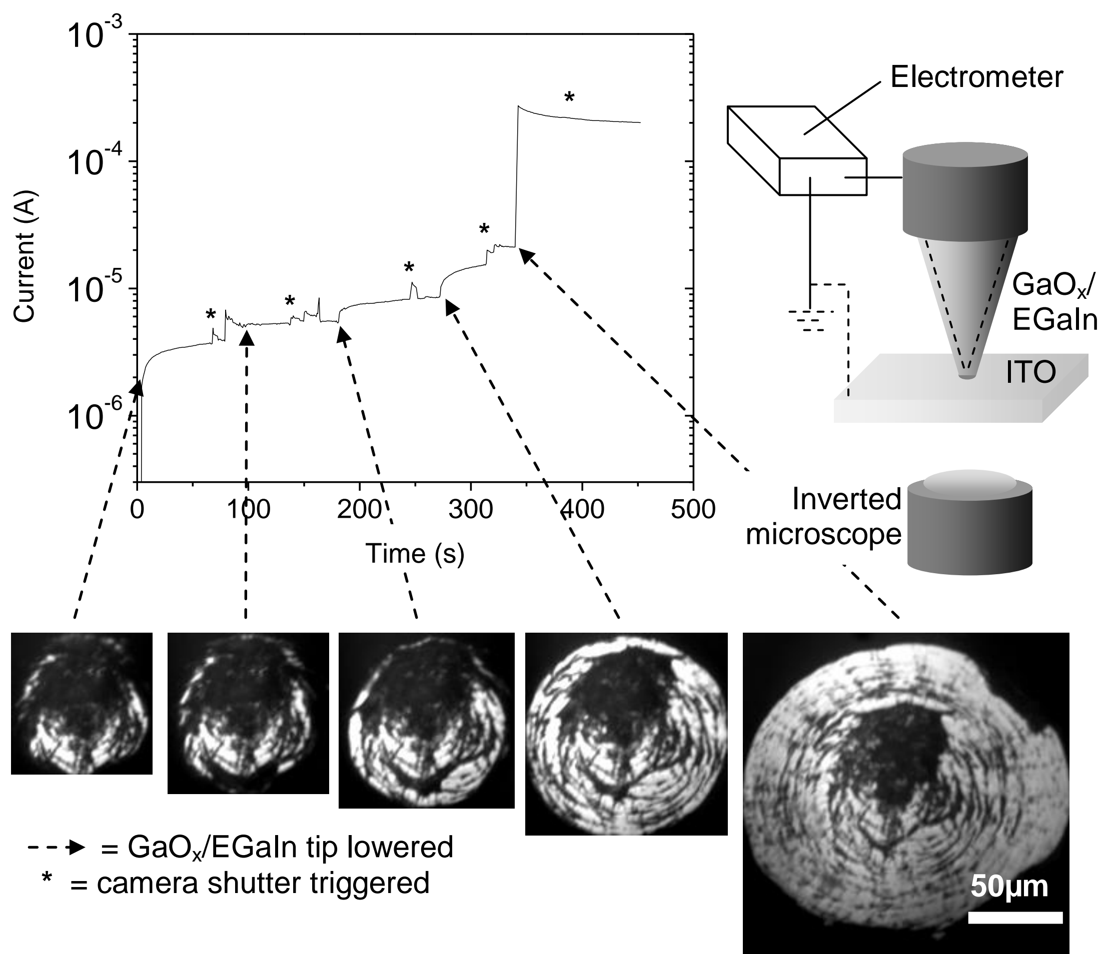

10^{-3}
10^{-4}
10^{-5}
10^{-6}
Current (A)
0
100
200
300
400
500
Time (s)
Electrometer
GaO_x/ EGaIn
ITO
Inverted microscope
50µm
= GaO_x/EGaIn tip lowered
* = camera shutter triggered

Figure S2: Current vs. applied bias at four temperatures in the range 295 K – 260 K for a Cu wire contacting the layer of Ga_2O_3 on the surface of a drop of EGaIn.

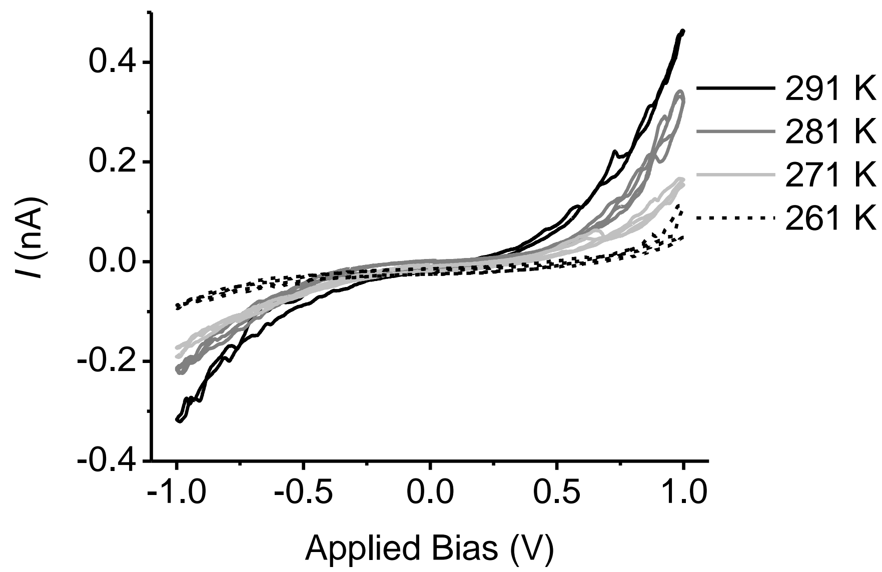
0.4
0.2
0.0
-0.2
-0.4
I (nA)
-1.0
-0.5
0.0
0.5
1.0
Applied Bias (V)
291 K
281 K
271 K
261 K

Microchannels on Glass Filled with Ga_2O_3/EGaIn. We fabricated microchannels in PDMS on glass surfaces to determine if the Ga_2O_3/EGaIn in the microchannels forms conformal contact with the bottom of the microchannels, i.e., the glass surface, and to test the following hypothesis. We hypothesize that during filling of the channels with EGaIn, the surface area of the Ga_2O_3/EGaIn increases and that the Ga_2O_3 layer ruptures exposing Ga atoms. These Ga atoms react with O_2 present in the microchannel to form Ga_2O_3. We believe that the microchannel does not contain enough O_2 to react with all exposed Ga surface atoms. Consequently, at least in a small part of our tunneling junctions, bulk EGaIn may form direct contact with the SAMs.

Figure S3A shows a microchannel in PDMS (oxidized for 30 s in a plasma of air, 500 mTorr) sealed on a glass surface (cleaned in a plasma of air for 5 min, 500 mTorr) filled with Ga_2O_3/EGaIn. We filled the microchannel with Ga_2O_3/EGaIn using the same procedure as described for the devices in the article. Figure S3A shows an optical micrograph of a channel filled with Ga_2O_3/EGaIn recorded through the bottom of the channel, i.e., the glass substrate. The optical micrograph shows that the Ga_2O_3/EGaIn fills the channel completely, forms stable structures, and makes a smooth and conformal contact with the glass surface.

Figure S3B shows an optical micrograph of the same microchannel after we removed the EGaIn from the microchannel by applying vacuum to the inlet of the microchannel. This optical micrograph shows that the EGaIn can be removed from the channel, but not all of it. We have reported that Ga_2O_3 interact strongly with glass surfaces.[5] We believe that the layer of Ga_2O_3 with some EGaIn sticks to the glass surface and is left behind in the microchannel. This experiment indicates that a layer of Ga_2O_3 between the glass surface and the EGaIn forms during

filling of the channel, but this layer is discontinuous; bulk EGaIn forms direct contact with the glass surface.

We estimated of the amount of O_2 in the microchannel to be 6.4×10^{-11} mol of O_2 (the volume of the channel is $8000 \times 30 \times 30$ μm^3, 7.2×10^6 μm^3, or 7.2×10^{-9} L and 1 mol of O_2 has a volume of 22.4 L) at ambient pressure. We filled the channel within 0.1 s (therefore we neglected diffusion of O_2 through the PDMS into the channel during filling) and during filling we increased the surface area of the EGaIn by 1×10^6 μm^2 ($4 \times 8000 \times 30$ μm^2) or 1×10^{-2} cm^2. The surface of EGaIn contains ~5×10^{15} Ga atoms per cm^2, thus we exposed about 8×10^{-11} mol Ga atoms to oxygen during filling of the microchannel. It seems, indeed, that there is not enough oxygen present during filling to react with all Ga atoms at the surface during filling of the microchannels with EGaIn by applying vacuum.

To ensure an environment that contains insufficient oxygen to react with the newly exposed Ga surface atoms during filling of the microchannels, we filled the microchannels with EGaIn under an atmosphere of N_2. We kept the assembled microchannels in a glove box with an atmosphere of N_2 for 24 h before we filled the channels inside the glove box with EGaIn. Figure S3C shows a channel filled with EGaIn under an atmosphere of N_2. The EGaIn did readily fill the channel, but the optical micrograph shows that it did not form stable structures and partially retracted form the channel, and did not form continuous structures. This behavior is similar to that observed for Hg in channels.5 Hg also readily fills microchannels, but it does not from stable features inside channels and retracts to minimize interfacial free energy once the pressure is relieved.5

These experiments indicate that we form a layer of Ga_2O_3 between the glass surface and the EGaIn, but that this layer is not continuous due to the lack of O_2 present in the microchannel.

Bulk EGaIn is, thus, in direct contact with the glass surface. Thus, in our SAM-based junctions the layer of Ga_2O_3 between the SAM and the bulk EGaIn may not be continuous and bulk EGaIn may form direct contact with the SAM.

These observations also confirm our previous conclusion5 that a layer Ga_2O_3 is responsible for the fact that Ga_2O_3/EGaIn behaves like an elastic material until it experiences a critical surface stress (~0.5 N/m), at which point it yields and flows readily. This property of Ga_2O_3/EGaIn makes it possible to fill microchannels rapidly when sufficient vacuum is applied to the outlet of the channel and it maintains structural stability within the channels once ambient pressure is restored to ambient. The microchannels can also be filled with Hg, but once ambient pressure is restored, Hg retracts from the microchannels. Thus, we did not try to fabricate our devices under an atmosphere of N_2 since the EGaIn top-electrodes do not form stable, continuous structures in the microchannels.

Figure S3: A) Optical micrographs of a microchannel in PDMS sealed against a glass surface filled with Ga_2O_3/EGaIn imaged through the glass surface (A), and after removal of the EGaIn (B). C) Optical micrograph of a channel filled with EGaIn under an atmosphere of N_2.

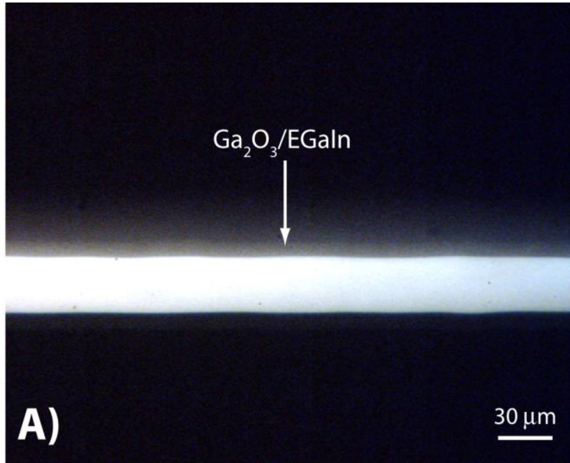
Ga_2O_3/EGaIn
A)
30 μm

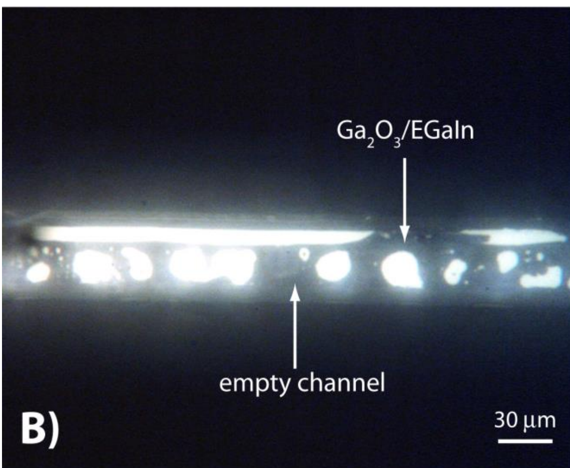
Ga_2O_3/EGaIn
empty channel
B)
30 μm

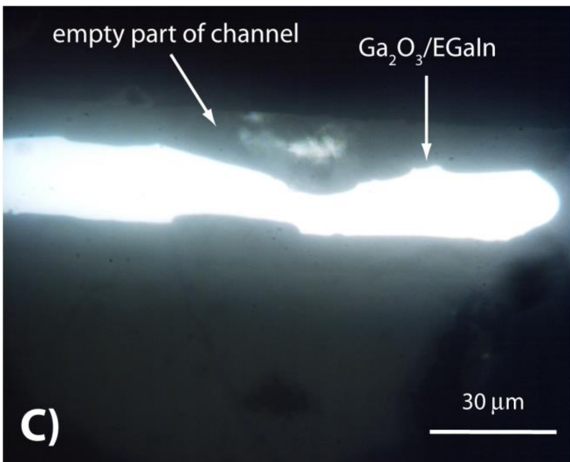
empty part of channel
Ga_2O_3/EGaIn
C)
30 μm

Wet Electrochemistry. We have reported our electrochemical analysis of the SAMs of $SC_{11}Fc$ SAMs before,2 but we give a brief description here. The $SC_{11}Fc$ SAMs were characterized at Au^{TS} electrodes by wet electrochemistry.[6,7] Electrochemical measurements were performed with an AUTOLAB PGSTAT10. A custom built three-electrode setup equipped with a platinum counter electrode, a Ag/AgCl reference electrode and a screw cap holding the gold working electrode (area exposed to the solution = 0.44 cm^2) was used. Cyclic voltammograms were recorded in aqueous solutions of 1 M $HClO_4$, at voltages ranging from –0.1 and 0.9 V at scan rates of 0.050, 0.10, 0.20, 0.50, 1.0, 2.0 and 5.0 V/s.

Figure S4 shows cyclic voltammograms of SAMs of $SC_{11}Fc$ on Au^{TS} electrodes formed over short (10 min) and long (24 h) periods of time measured with different scan rates. We calculated the the surface coverage of the Fc units (Γ_{Fc} = mol/cm^2) using eq. **S1**, where n = the number of electrons per mole of reaction, F is the Faraday constant, and A is the surface area of the electrode exposed to the electrolyte solution (0.44 cm^2)[8]:

$$\Gamma_{Fc} = Q_{tot}/nFA \qquad \textbf{(S1)}$$

Integration of the cyclic voltammogram gives the total charge (Q_{tot}) of $2.1 \times 10^{-5} \pm 0.2 \times 10^{-5}$ C, which we found to be independent on the scan rate as expected for a surface confined redox-reaction.8 Using eq. **S1** gives $\Gamma_{Fc} = 4.9 \pm 0.4 \times 10^{-10}$ mol/cm^2, which is close to the theoretical value $\Gamma_{Fc} = 4.5 \times 10^{-10}$ mol/cm^2 calculated assuming a hexagonal packing, with Fc is treated as spheres with a diameter of 6.6 Å.[9]

The energy level for the HOMO (E_{HOMO}) was estimated to be ~ -5.0 eV, relative to vacuum, using eq. **S2**, where $E_{abs,NHE}$ is the absolute potential energy of the normal hydrogen electrode (-

4.5 eV), and $E_{1/2,\mathrm{NHE}}$ is the formal half-wave potential vs normal hydrogen electrode which is 0.466 eV:

$$E_{\mathrm{HOMO}} = E_{\mathrm{abs,NHE}} - eE_{1/2,\mathrm{NHE}} \qquad \textbf{(S2)}$$

The shape of the cyclic voltammogram gives qualitative information about the structure of the SAMs of $SC_{11}Fc$. Symmetrical cyclic voltammograms are obtained for disordered or diluted SAMs with Fc termini give symmetrical cyclic voltammograms; this shape indicates a single reversible electrochemical process. Cyclic voltammograms with broad waves, or even multiple oxidation events, and with the oxidation peak shifted toward higher positive potentials are obtained when the SAMs are densely packed; this shape indicated multiple oxidation events which are related to strongly interacting Fc moieties that are located in the top of the SAMs.

For SAMs formed over 24 h, we observed a single oxidation wave when we used high scan rates (> 0.50 V/s; Fig. S4A). For SAMs formed over only 10 min, two oxidation waves appeared in the cyclic voltammograms (Fig. S4C). At low scan rates we always observed two waves (Fig. S4B). The wave at higher oxidation potentials is dominant. These observations suggest that the SAMs are densely packed and have a low number of defects. Additionally, the small difference between the peak cathodic and peak anodic potentials (E_{pc} and E_{pa}, respectively), which increases with increasing scan rate, suggests slow electron transfer processes due to the presence of the long alkyl chains and order in the SAM.[10] The Fc groups may be buried in the SAM (back-bending) resulting in a third oxidation wave at higher oxidation potentials than the first two waves.[11] We do not observe a third oxidation wave from which we conclude that the SAMs of $SC_{11}Fc$ have the Fc moieties separated from the electrode by the SC_{11} groups.

Figure S4: Cyclic voltammograms of SAMs of $SC_{11}Fc$ on Au. The SAMs were formed for 24 h (A and B) or 10 min (C) using a 1 mM ethanolic solutions of $HSC_{11}Fc$ at R.T. under an argon atmosphere (aqueous 1 M $HClO_4$ as electrolyte solution, and potentials vs. Ag/AgCl); A) scan rate = 2.0, 1.0, and 0.50 V/s; B) scan rate = 0.200, 0.100, and 0.050 V/s,); C) scan rate = 2.0, 1.0, 0.50, 0.200, 0.100, and 0.050V/s.

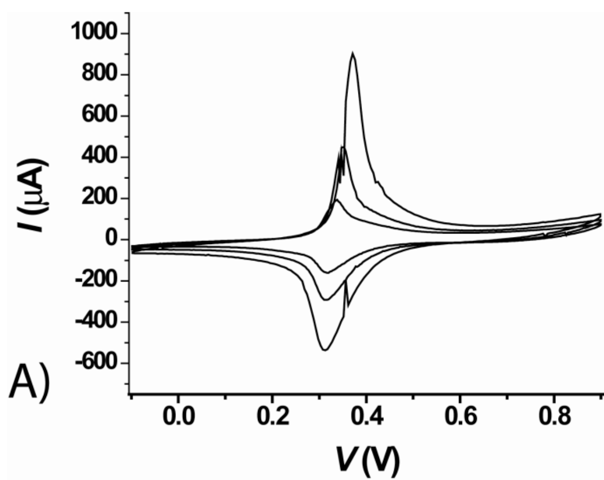
1000
800
600
400
200
0
-200
-400
-600
I (μA)
A)
0.0
0.2
0.4
0.6
0.8
V (V)

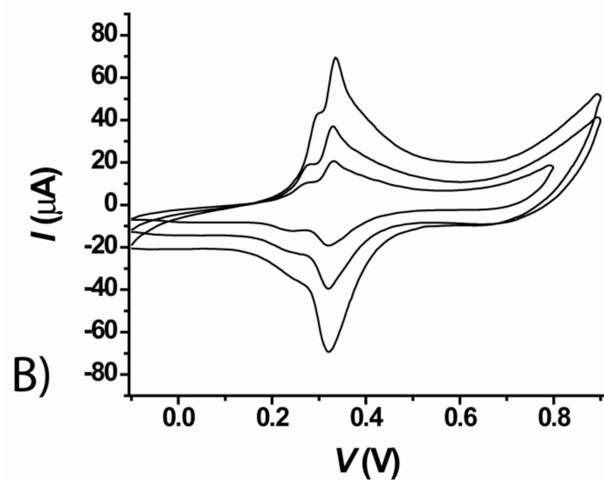
80
60
40
20
0
-20
-40
-60
-80
I (μA)
B)
0.0
0.2
0.4
0.6
0.8
V (V)

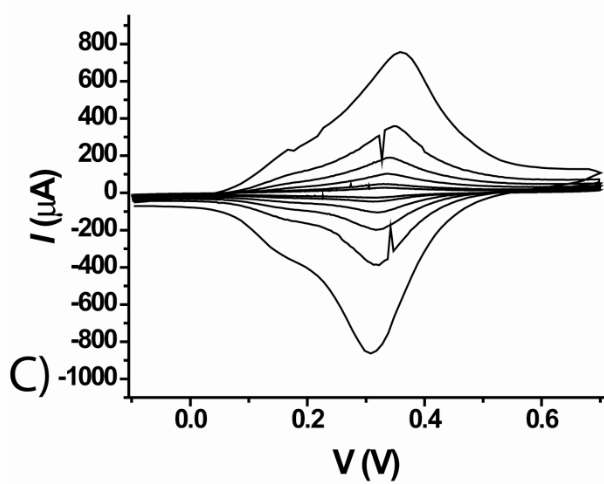
800
600
400
200
0
-200
-400
-600
-800
-1000
I (μA)
C)
0.0
0.2
0.4
0.6
V (V)

Data Collection and Statistical analysis. Table S1 summarizes the numbers of junctions and substrates that we measured, and the yields of working devices. Typically, we prepared 2 – 6 devices of each type of SAM and measured 21 *J*(V) traces (one trace = 0V → +0.5V → -0.5V → 0V at steps of 50 mV with a delay of 0.50 s) from each junction on all devices with SAMs of $SC_{n-1}CH_3$.

We constructed histograms of all values of *J* for all potentials that we measured. The values of *J* have a log-normal distribution. To these histograms we fitted Gaussian functions to obtain the mean value of *J* and the log-standard deviation, which, in turn, were used to construct the average *J*(V) curves. We used only single Gaussians to fit all data. We did not select or remove data prior to fitting. The non-linear least-squares fitting procedure resulted in a best fit centered on the main peak in the histogram (see below).

Figure S5 shows the average *J*(V) curves (the error bar represents one log-standard deviation), and histograms, with Gaussian fits to these histograms, of the values of *J* measured at -0.2 V and -0.5 V of the Ag^{TS}-$SC_{n-1}CH_3$//Ga_2O_3/EGaIn junctions with n = 12, 14, 16, or 18.

Table S1: Statistics of the Ag^{TS}-SAM//Ga_2O_3/EGaIn junctions.

Junction	Number of Devices	Number of Junctions	Shorts	Open Circuits	Yield (%)	Total Scans
$SC_{11}CH_3$	3	21	9	2	48	400
$SC_{13}CH_3$	2	14	2	2	71	400
$SC_{15}CH_3$	4	28	5	1	79	631
$SC_{17}CH_3$	3	21	3	-	86	756
$SC_{11}Fc$	5	35	4	1	86	238

Figure S5: The log-average *J*(V) curves with the error bars indicating the log-standard deviation of junctions composed of SAMs of $SC_{11}CH_3$ (A), $SC_{13}CH_3$ (D), $S_{15}CH_3$ (G), and S_{17} CH_3 (J). The histograms of the values of *J* measured at -0.20 or -0.50 V, with Gaussians fits to these histograms, for junctions with SAMs of $SC_{11}CH_3$ (B and C), $SC_{13}CH_3$ (E and F), $S_{15}CH_3$ (H and J), and $S_{17}CH_3$ (K and L).

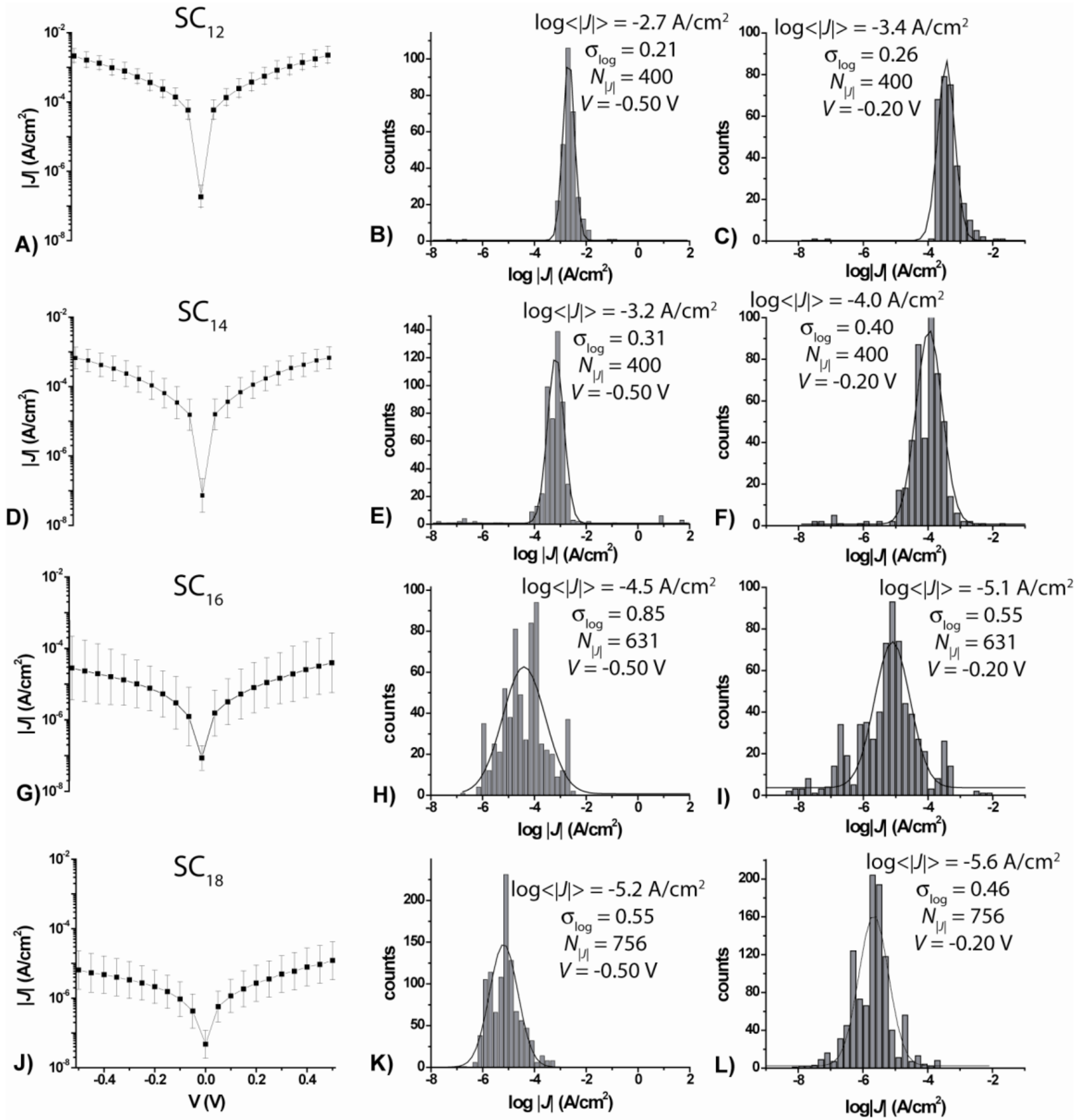
SC$_{12}$
A)
log<|J|> = -2.7 A/cm^2
σ_{log} = 0.21
$N_{|J|}$ = 400
V = -0.50 V
B)
log<|J|> = -3.4 A/cm^2
σ_{log} = 0.26
$N_{|J|}$ = 400
V = -0.20 V
C)
SC$_{14}$
D)
log<|J|> = -3.2 A/cm^2
σ_{log} = 0.31
$N_{|J|}$ = 400
V = -0.50 V
E)
log<|J|> = -4.0 A/cm^2
σ_{log} = 0.40
$N_{|J|}$ = 400
V = -0.20 V
F)
SC$_{16}$
G)
log<|J|> = -4.5 A/cm^2
σ_{log} = 0.85
$N_{|J|}$ = 631
V = -0.50 V
H)
log<|J|> = -5.1 A/cm^2
σ_{log} = 0.55
$N_{|J|}$ = 631
V = -0.20 V
I)
SC$_{18}$
J)
log<|J|> = -5.2 A/cm^2
σ_{log} = 0.55
$N_{|J|}$ = 756
V = -0.50 V
K)
log<|J|> = -5.6 A/cm^2
σ_{log} = 0.46
$N_{|J|}$ = 756
V = -0.20 V
L)
|J| (A/cm^2)
V (V)
counts
log |J| (A/cm^2)
log|J| (A/cm^2)

Non-Zero Current at Zero Bias. We observed a small current (~10^{-8} – 10^{-7} A/cm^2; Figure S6), and changed (by one order of magnitude) from measurement to measurement, near zero bias in all J(V) measurements of the Ag^{TS}-$SC_{11}Fc$//Ga_2O_3/EGaIn junctions. Figure S6A shows, on a linear scale, ten J(V) curves of one representative junction – that is, a junction with its J(V) characteristics within one log-standard deviation from the log-mean value of J for the entire dataset – of a Ag^{TS}-$SC_{11}Fc$//Ga_2O_3/EGaIn junction measured at ± 1.0 V. Fig. S6B shows the same J(V) curve as in Fig. S6A at potentials between -0.5 and 0.5 V. Fig. S6C shows the same data on a semi-log plot; we normally report the absolute values of |J/ on a logarithmic scale. The small current near zero bias discussed above causes the semi-log plots to appear to have anomalies close the origin.

Figure S6: Ten *J*(V) curves of a single Ag^{TS}-$SC_{11}Fc//Ga_2O_3$/EGaIn junction measured between ±1.0 V (A) and an expanded section (B). In C) shows the corresponding |*J*|(V) curve. The arrows indicate the direction of the scan.

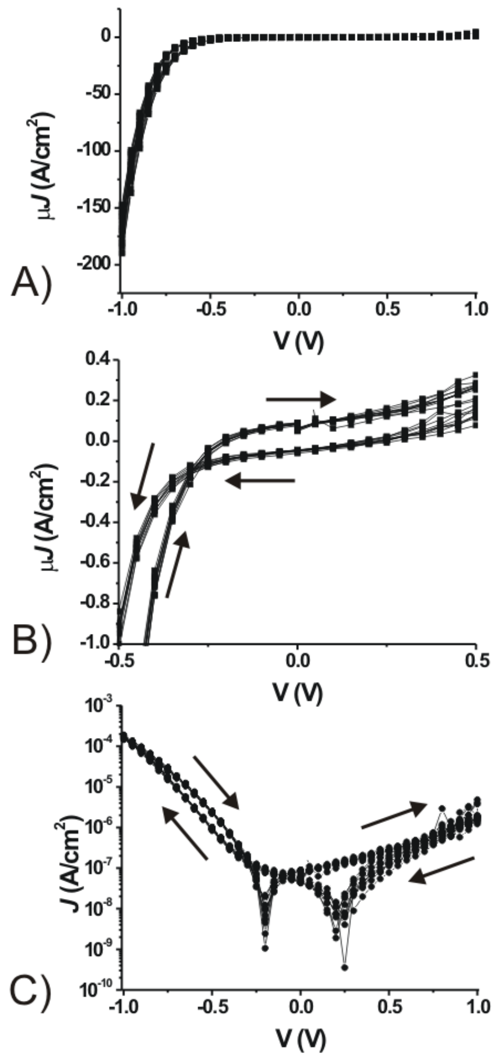

A)
μJ (A/cm²)
0
-50
-100
-150
-200
-1.0
-0.5
0.0
0.5
1.0
V (V)
B)
μJ (A/cm²)
0.4
0.2
0.0
-0.2
-0.4
-0.6
-0.8
-1.0
-0.5
0.0
0.5
V (V)
C)
J (A/cm²)
10⁻³
10⁻⁴
10⁻⁵
10⁻⁶
10⁻⁷
10⁻⁸
10⁻⁹
10⁻¹⁰
-1.0
-0.5
0.0
0.5
1.0
V (V)

Fitting Log-Normally Distributed Data with Gaussians. Our data for J and R are approximately log-normally distributed, meaning that log(/J/) and log(R) are both normally distributed. The following description of our procedure for fitting J also applies to the distributions of R. To fit a observed log-normal distribution of J at a certain voltage, we created histograms of log(|J|); this distribution has the appearance of a normal distribution. We then used a trust-region algorithm (available in the curve-fitting toolbox of MATLAB 7.4.0.287, R2007a) to minimize the function **S4** (nonlinear least-squares fitting) where **x** is a vector representing the centers of the logarithmically-spaced bins in the histogram, **y** is the vector of counts in the histogram (i.e., $\mathbf{y}_i$ is the number values of log(|J|) that fall within bin i, centered at $\mathbf{x}_i$).[12]

$$F(\mathbf{x}) = \|\mathbf{y} - G(\mathbf{x})\|^2 \qquad \textbf{(S4)}$$

The G(**x**) is the Gaussian function, given by **S5** where m is the mean and s is the standard deviation of log(|J|).

$$G(\mathbf{x}) = \frac{1}{s\sqrt{2\pi}} \exp\left(-\frac{(\mathbf{x}-m)^2}{2s^2}\right) \qquad \textbf{(S5)}$$

To report statistics for |J|, we calculate the log-mean, $\mu_{\log} = 10^m$, and log-standard deviation, $\sigma_{\log} = 10^s$, of |J|. Because log(|J|) is normally distributed, 68% of its distribution lies within the interval (m-s, m+s); however, since |J| is log-normally distributed, 68% of its distribution lies within the interval ($\mu_{\log}/\sigma_{\log}$, $\mu_{\log}\times\sigma_{\log}$), or equivalently, ($10^{m-s}$, 10^{m+s}).

Statistical Analysis of the Rectification Ratio. In Figure 3C we fitted all data to a single Gaussian using a non-linear least-squares fitting procedure. This fit looks to the eye

unsatisfactory, and it seems that data have been excluded from the fit. The opposite, however, is true; none of the data have been excluded. The data that seem to be excluded do not weigh in the fitting as much as the data centered close to the main peak. Figure S7 shows the same data as do Figure 3C, but with two Gaussians fitted to this histogram. The smaller of the two Gaussians represent 20 counts; all of these originated from one instable junction. The mean value of R (obtained from the larger Gaussian) is not significantly different ($R \approx 1.3 \times 10^2$) than that of obtained by fitting the histogram to a single Gaussian ($R \approx 1.3 \times 10^2$).

Figures S7: The histogram of the rectification ratios of the obtained for devices with SAMs of $SC_{11}Fc$ with two Gaussian fitted to this histogram.

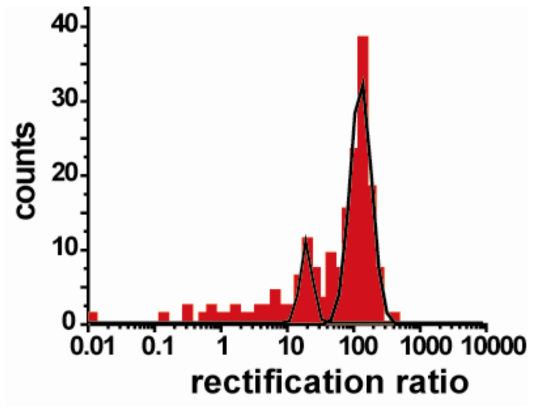
40
30
20
10
0
counts
0.01
0.1
1
10
100
1000
10000
rectification ratio

References

[1] Holmlin, R. E.; Haag, R.; Chabinyc, M. L.; Ismagilov, R. F. Cohen, A. E.; Terfort, A.; Rampi, M. A.; Whitesides, G. M. J. *J. Am. Chem. Soc.* **2001**, *123*, 5075.

[2] Nijhuis, C. A; Reus, W. F.; Whitesides, G. M. *J. Am. Chem. Soc.* **2009**, *131*, 17814.

[3] Paterson, G. W.; Wilson, J. A.; Moran, D.; Hill, R.; Long, A. R.; Thayne, I.; Passlack, M.; Droopad, R. *Mater. Sci. Eng. B*, **2006**, *135*, 277.

[4] Reus, W. F.; Nijhuis, C. A.; Whitesides, G. M. et al. unpublished results.

[5] Dickey, M. D.; Chiechi, R. C.; Larson, R. J.; Weiss, E. A.; Weitz, D. A.; Whitesides, G. M. *Adv. Funct. Mater.* **2008**, *18*, 1097.

[6] Auletta, T.; van Veggel, F. C. J. M.; Reinhoudt, D. N. *Langmuir* **2002,** *18,* 1288.

[7] Chidsey, C. E. D.; Bertozzi, C. R.; Putvinski, T. M.; Mujsce, A. M. *J. Am. Chem. Soc.* **1991**, *112*, 4301.

[8] Bard, A. J.; Faulkner, L.R. *Electrochemical Methods: Fundamentals and Applications* John Wiley & Sons: New York, **2001**.

[9] Rowe, G. K.; Creager, S. E. *Langmuir* **1991,** *7*, 2307.

[10] Weber, K.; Hocket, L.; Creager, S. *J. Phys. Chem.* **1997**, *101*, 8286.

[11] Auletta, T.; van Veggel, F. C. J. M.; Reinhoudt, D. N. *Langmuir* **2002,** *18,* 1288.

[12] We obtained Gaussian fits using a least-squares, trust-region based algorithm: the 'gauss1' model (all options set to default) in the curve-fitting toolbox in MATLAB 7.4.0.287 (R2007a) Copyright The MathWorks, Inc. 1984-2007. No weighting or exclusion rules were applied to the data.